Vibrational Spectra of *N*,*N*-Dimethylaniline and Its Radical Cation. An Interpretation Based on Quantum Chemical Calculations

A. M. Brouwer*,† and R. Wilbrandt*,‡

Amsterdam Institute of Molecular Studies, Laboratory of Organic Chemistry, University of Amsterdam, Nieuwe Achtergracht 129, NL-1018 WS Amsterdam, The Netherlands, and Department of Environmental Science and Technology, Risø National Laboratory, MIL-313, DK-4000 Roskilde, Denmark

Received: January 2, 1996; In Final Form: March 26, 1996[⊗]

The resonance Raman spectrum of the radical cation of *N*,*N*-dimethylaniline (DMA) has been remeasured, and different types of ab initio calculations have been performed to interpret the vibrational spectra of this species and the deuteriated isotopomers previously studied by Poizat et al. (*J. Chem. Phys.* **1989**, *90*, 4697). Density functional methods (UBLYP/6-31G*) give results superior to those of Hartree−Fock calculations for the vibrational frequencies of the radical cation of DMA. The same level of theory was also successfully applied to the vibrational spectrum of aniline. CASSCF calculations were used to study the potential energy surfaces of the lowest excited states of the radical cation of DMA, allowing the estimation of resonance Raman intensities. For the neutral DMA conventional HF/6-31G* calculations allow a straightforward interpretation of the infrared and Raman spectra. The calculations lead to revision of some of the previous empirical assignments.

1. Introduction

The amino group holds a special position in organic chemistry because it is the simplest and most readily available electron-rich functional group. The lone pair electrons give amines important chemical reactivity, as a base, as a nucleophile, or as an electron donor. In the latter role amines have been frequently used in the field of photoinduced electron transfer, from its earliest stages[1,2] up to the present days.[3−8] In relation to our studies of polyamino electron donor−acceptor systems,[5,6,8] we are interested in the interactions between the amino groups in the different charge-separated excited states that can exist in such multicomponent systems. For comparison, the corresponding radical cation species containing two (or more) donor groups have been studied recently by optical absorption and resonance Raman spectroscopy.[5,9]

The purpose of the present paper is to provide a strong foundation for the interpretation of the vibrational spectra of radical cations of more complicated aromatic amines by focusing first on *N*,*N*-dimethylaniline (DMA). This compound is small enough to be well suited for quantum chemical investigation, and much is known about it experimentally. Radical cations of aniline derivatives are intermediates in various chemical processes in the liquid phase and have been studied by electrochemical methods,[10] magnetic resonance,[11−13] optical absorption,[14−17] and resonance Raman spectroscopy.[18−23] Vibrational data of the radical cation states of the isolated aniline molecule have been recently obtained using photoelectron spectroscopic techniques.[24,25]

For the interpretation of the vibrational spectra of radicals and radical cations of simple substituted benzenes such as benzyl,[26] aniline,[24] phenylenediamine,[27] and phenoxyl,[28] various levels of ab initio quantum chemical theory have been applied. Our goal in the present study is to establish an acceptable level of calculation for the radical cation of *N*,*N*-dimethylaniline (DMA^+), for which extensive resonance Raman data are available.[22] The theoretical method should not be too computationally demanding, because we intend to apply the same approach later to larger systems. After we found that density functional theory (DFT) calculations (section 3.2) give excellent results for DMA^+, we briefly investigated the aniline radical cation, with equally good results (section 3.3). During the study we were surprised to see that the typical ring mode 6a was not reported by the Poizat group[22] for the parent isotopomer of DMA^+, and therefore we remeasured the spectrum of this species. The results that we present here will serve as a firm basis for the interpretation of the spectra of radical cations of more complicated aniline derivatives, in particular piperidines and piperazines.[29]

2. Experiments

Excitation at 308 nm or at shorter wavelengths of aniline derivatives in polar solvents leads to the formation of triplets and radical cations.[22,30] The former are readily quenched in air-saturated solvent. Thus, the DMA radical cation was generated by exciting a 5×10^{-4} M aerated solution in acetonitrile at 248 nm (Lambda Physik LPX 220i Excimer laser, 9 mJ, 20 ns pulses). Resonance Raman spectra were excited 70 ns after the photolyzing light pulse, at a wavelength of 465 nm, with pulses of 1.0−2.0 mJ/pulse energy (15 ns pulses, 5 Hz repetition rate) from an excimer (Lambda Physik EMG102E) pumped dye laser (Lambda Physik FL3002). Scattered Raman light was collected at right angles to the laser beam, passed through a bandpass filter (Schott GG475) and a polarization scrambler, and dispersed in a home-built 0.6 m spectrograph. The spectral resolution was 8 cm^{-1}. Spectra were detected by a gated intensified optical multichannel analyzer (Spectroscopy Instruments OSMA IRY-700) with 700 active channels. The wavenumber scale was calibrated using the Raman spectrum of indene as a reference. Data handling was performed on a PDP11/23 computer. A sample was exposed to 250 laser pulses, and spectra from four samples were averaged. The final spectra were obtained after subtraction of solvent bands. The spectra were not corrected for the absorption of the GG475 filter, the absorption of the sample, and the wavelength dependence of the sensitivity of our detection system.

† University of Amsterdam.
‡ Risø National Laboratory.
⊗ Abstract published in *Advance ACS Abstracts,* May 1, 1996.

S0022-3654(96)00013-5 CCC: $12.00

In addition to the experiments on the radical cation of DMA, we also attempted to obtain the resonance Raman spectrum of the T_1 state. This was generated by excitation of a 2 mM solution of DMA in argon-deoxygenated cyclopentane at 308 nm. Although the triplet state is known to be formed efficiently (rate of intersystem crossing 4×10^8 s^{-1}, triplet yield ca. 0.8,[31,32] and the absorption is in the same spectral region (460 nm, $\epsilon =$ 4000 M^{-1} cm^{-1})[30] and of about the same strength as that of the radical cation[14−16]), we could not detect significant Raman scattering of this species. This result is in contrast with those for some *N*-phenylpiperidine and *N*-phenylpiperazine derivatives, which gave weak but detectable transient resonance Raman spectra under the same conditions.[29]

3. Assignment of Spectra

3.1. Neutral DMA. The Raman and IR spectra of the neutral ground state of DMA and three of its deuteriated isotopomers have been reported by Guichard et al.[33] and assigned on the basis of a previous analysis.[34] Recently, the vibrational spectra of aniline were analyzed in detail[35] on the basis of semiempirical and ab initio calculations. The IR spectrum of aniline was also recently studied using density functional methods.[36]

We shall in the following briefly present the results of HF/6-31G* ab initio calculations[37] on DMA-d_0, DMA-d_6, DMA-d_5, and DMA-d_{11} in their neutral ground states and compare the results with the experimental data of Guichard et al.[33] and their assignments. The symmetry of DMA in its neutral ground state is C_s with the nitrogen being pyramidalized and the two methyl groups being slightly tilted out of the plane of the phenyl ring (see section 4.1). This is qualitatively similar to aniline.

The observed Raman and IR spectra reported by Guichard et al.[33] [GBLP] are listed in Table 1 together with our calculations and assignments. We have adopted the conventional procedure[38] of scaling the computed harmonic frequencies by a factor of 0.9 to correct for deficiencies of the Hartree−Fock method and for differences between harmonic and observed 0→1 transition frequencies. IR and Raman intensities were calculated but are not listed.

In general, the calculations reproduce the observed spectra of the four isotopomers very satisfactorily, and the agreement with the previous empirical assignment of GBLP is in general good. However, a few points should be mentioned. For many modes deuteriation changes the coupling pattern between ring modes and vibrations of the dimethylamino group substantially. It is therefore in some cases difficult to draw a straightforward correlation between modes of the various isotopomers. We shall in the following discuss the assignment derived on the basis of the present theoretical results. Unless stated differently, calculated bands refer to DMA-d_0.

The frequency of the 8a mode is well reproduced for all isotopomers, and the assignments are in agreement with GBLP. While this mode is weakly coupled with a methyl deformation mode for DMA-d_0 and DMA-d_5, in DMA-d_6 and DMA-d_{11} the methyl vibration is shifted to lower wavenumbers and the 8a mode is in these cases a pure ring mode. Mode 8b, observed only in IR, is a pure ring mode and well reproduced by calculations for all isotopomers.

The assignment of the 19a mode is in general agreement with GBLP, judging on the basis of the ring displacements only. However, it should be noted that for DMA-d_5 and DMA-d_{11}, this mode has its strongest contribution from the C−N stretching coordinate, in additon to the ring displacements (see below). Furthermore, it is strongly coupled with a methyl deformation in DMA-d_0 and DMA-d_5.

A series of bands calculated at 1498, 1483, and 1477 cm^{-1} are due to methyl deformations and assigned in general agreement with GBLP. Also, the symmetric "umbrella" methyl deformation (calculated at 1474 cm^{-1}) and its antisymmetric counterpart (calculated at 1437 cm^{-1}) are assigned in agreement with GBLP, apart from the band at 1130 cm^{-1} in DMA-d_{11}, which more likely is due to the 18b mode. As the region from 1067 to 1091 cm^{-1} in DMA-d_{11} is rather crowded, assignments in this region are uncertain. Methyl rock modes are predicted at 1169, 1133, 1119, and 1057 cm^{-1}. Of these, the 1133 cm^{-1} band is the symmetric rock mode. Our assignments are in qualitative agreement with GBLP.

Ring mode 3, calculated at 1352 cm^{-1}, is assigned to the observed bands at 1335/1340 cm^{-1} in DMA-d_0, at 1320 cm^{-1} in DMA-d_6, and at 1036 cm^{-1} in DMA-d_5. GBLP assign some of these bands (1335/1340 and 1320 cm^{-1}) incorrectly to mode 14, which according to our calculations is predicted at 1189 cm^{-1}.

The frequency of the N-ring stretching vibration is sensitive to deuteriation of the ring and of the methyl groups. The ν(N-ring) vibration is calculated at 1338 cm^{-1} for DMA-d_0. This mode is a strongly mixed mode with contributions from methyl deformations and CH bending (19a). In DMA-d_6 it is shifted by 25 cm^{-1} to 1313 cm^{-1} according to calculations and the methyl contribution is reduced. Experimentally, the shift is much smaller. In DMA-d_5, the mode with the strongest ν(N-ring) contribution is the one calculated at 1399 cm^{-1}, assigned above to mode 19a; however, a considerable ν(N-ring) contribution is also calculated for the 1295 cm^{-1} band. Also in DMA-d_{11}, two modes at 1256 and 1401 cm^{-1} show strong ν(N-ring) contributions giving rise to an in-phase and out-of-phase combination of ν(N-ring) with mode 19a. GBLP did consider only one of these two modes in DMA-d_5 and DMA-d_{11}, respectively.

While the antisymmetric $\nu(NC_2)$ mode is calculated at 1272 cm^{-1} and assigned in agreement with GBLP for all isotopomers, the symmetric $\nu(NC_2)$ mode couples according to calculations with ring mode 1, giving rise to in-phase and out-of-phase combinations at 725 and 934 cm^{-1}. Such a coupling is apparent in DMA-d_0, DMA-d_6, and DMA-d_5.

Ring mode 18a, predicted at 1026 cm^{-1}, couples with CD_3 rock in DMA-d_6 and DMA-d_{11}. Mode 18b, predicted at 1096 cm^{-1}, couples with CH_3/CD_3 rock in DMA-d_o and DMA-d_5 and with methyl deformations in DMA-d_{11}. This leads to revised assignments for the bands observed at 1135/1132 cm^{-1} in DMA-d_5, compared with GBLP.

In the low-frequency region below 1000 cm^{-1} one finds ring modes 5, 17a, 12, 1, 17b, 10a, 11, 4, 6b, 16b, and 16a and the stretching and bending modes of the dimethylamino group. Most of the assignments proposed by GBLP are in qualitative agreement with the present calculations, although some of the modes have more mixed character.

In summary, the present calculations are in excellent agreement with the observed data of GBLP[33] and provide a firm basis for the assignment of most of the observed bands in all four isotopomers. The only unassigned observed bands are two weak bands at 1300 cm^{-1} in DMA-d_5 and at 1295 cm^{-1} in DMA-d_{11}.

3.2. Radical Cation of DMA. The resonance Raman spectra of the radical cation of *N*,*N*-dimethylaniline (DMA^+) and several isotopomers have been reported and assigned a few years ago by the Poizat group.[22] This offers an ideal testing ground for different computational approaches. It will be found that DFT[39] using Becke's exchange functional[40] together with the LYP correlation functional[41] gives results that are clearly superior

TABLE 1: Observed[a] Vibrational Data and Calculated[b] Frequencies of DMA and Three of Its Isotopomers in the Neutral Ground State (C_s Point Group)

DMA								DMA-d_6						DMA-d_5						DMA-d_{11}					
Raman			IR		6-31G*	sym	assignment	Raman			IR		6-31G*	Raman			IR		6-31G*	Raman			IR		6-31G*
1605	s	0.3	1600	s	1627	a'	8a	1600	s	0.3	1598	s	1626	1575	s	0.3	1572	s	1588	1575	s	0.3	1570	s	1586
			1578	w	1598	a''	8b				1570	w	1598				1542	w	1558				1540	w	1557
			1508	s	1516	a'	19a, ν(N-ring)				1500	s	1510	1400	w	0.1	1396	s	1399	1421	w	0.1	1416	s	1401
					1514	a'	δCH_3						1090						1514						1091
					1498	a''	δCH_3						1080						1496						1082
1480	vw	dp	1480	sh	1483	a'	δCH_3						1072	1485	sh	dp	1482	m	1485	1070	w		1068	w	1072
					1477	a'	δCH_3						1065						1476	1060	sh		1057	w	1067
1450	w	0.45	1442	m	1474	a'	δCH_3	1136	w	0.4	1135	m	1155	1455	m		1456	w	1478	1138	w				1149
					1465	a''	19b						1464						1361						1356
1415	vw	dp			1437	a''	δCH_3	1055	sh	0.6	1060	w	1056	1415	w	dp			1439						1073
1335	sh		1340	sh	1352	a''	3	1320	sh		1320	sh	1354				1036	w	1038						1031
1348	m	0.1	1345	s	1338	a'	ν(N-ring), δCH_3	1343	w	0.1	1344	s	1313	1298	m	p	1294	s	1295	1275	m	p	1270	m	1256
																			1399						1401
			1230	m	1272	a''	$\nu(NC_2)$, δCH				1210	m	1247				1222	m	1256				1210	m	1236
1195	m	0.1	1190	m	1192	a'	9a	1193	w	0.1	1192	w	1194	874	m	0.1	870	w	869	875	m	0.1	872	vw	868
1165	sh	0.5	1166	m	1189	a''	14	1157	w	0.5	1150	w	1191	805	vw	0.7	805	w	827	810	w	0.6	806	m	826
1160	m	p	1160	sh	1169	a'	ρCH_3, ν(N-ring)	1022	m	0.02	1021	m	1011						1145	1024	m	0.05	1020	w	1004
1132	w	p	1130	w	1133	a'	ρCH_3	911	w	0.1	903	vw	901	1140	m	0.08	1138	m	1124	912	vw		905	w	900
					1119	a''	ρCH_3	865	vw		864	vw	851						1113	845	w	0.6	850	w	851
					1096	a''	18b, ρCH_3						1103	1135	sh	0.08	1132	sh	1143				1130	m	1146
					1082	a''							1096						838	835	sh	0.6	830	w	838
			1060	w	1057	a''	ρCH_3						830				1063	w	1058	825	sh		826	sh	829
1038	s	0.05	1030	w	1026	a'	18a, ρCD_3						1040	880	sh	0.09			828	880	sh	0.08			843
					1000	a'	5						999	835	w	0.6	830	w	832						832
					979	a''	17a						979						791						791
995	vs	0.1	992	m	970	a'	12	988	vs	0.06	987	w	970	964	vs	0.1	960	m	939	960	vs	0.1	956	w	937
949	m	0.05	943	m	934	a'	1, $\nu(NC_2)$	828	w	0.1	826	w	819	945	s	0.08	940	w	927						799
868	vw		863	w	888	a'	17b	865	vw		864	vw	887	752	vw		750	m	765	752	vw		748	m	763
812	w	0.6			828	a''	10a	808	vw	0.6			826	638	m	0.6			647	634	w	0.6			646
750	sh	dp	750	s	764	a'	11	749	w	0.6	749	s	762				628	w	635				628	w	634
744	s	0.1	744	sh	725	a'	1, $\nu(NC_2)$	715	m	0.1	715	w	702	707	s	0.1	703	w	693	688	m	0.1	686	w	672
			690	s	695	a'	4				690	s	693	552	w		550	m	551	552	vw		552	s	550
618	w	0.6			612	a''	6b	616	vw	0.7			611	595	w	dp			586	595	w	dp	590	vw	585
520	vw	0.6			542	a'	scissor NC_2, ρCH_3, ΔNC_2	489	w	0.7			490	520	sh				530	490	w	dp			487
			518	m	516	a'	16b				518	m	522	440	sh		438	sh	446	445	sh		443	m	444
470	w	0.7	475	sh	453	a''	βCN	437	w	0.7			426	455	w		459	vw	438	425	w	dp	425	sh	409
					414	a''	16a						414						363						362
400	w	0.5			398	a'	ΔNC_2	353	w	0.55			353	398	w	0.4			394	353	w	0.5			350
					286	a'	w(ring-NC_2)						267						276						256
					282	a''	$\tau(NC_2)$						244						275						238
					191	a''	$\tau(NCH_3)$						145						188						143
					172	a'	$\tau(NCH_3)$						132						169						129
					119	a'	wCH_3						108						115						106
					39	a''	τCN						35						37						34

[a] From Guichard et al.[33] [b] All calculated frequencies were scaled down by a factor 0.9.

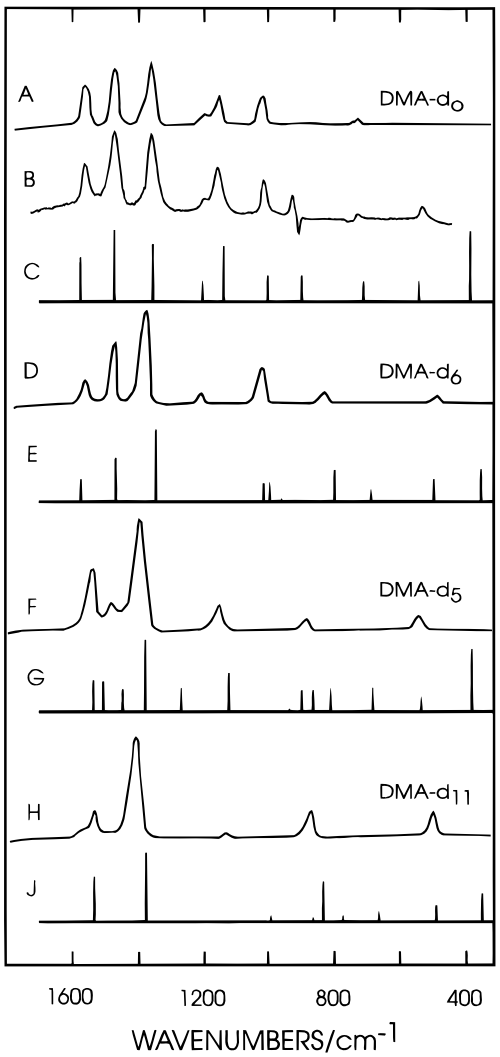

Figure 1. (A, B, D, F, H) Experimental resonance Raman spectra of isotopomers of DMA^+ [from ref 22, except for the d_0 isotopomer (this work, trace B)]. (C, E, G, J) Calculated resonance Raman spectra (see section 4.4).

to those obtained with Hartree−Fock (HF) methods. Therefore, we shall present the results of the DFT calculations first and then briefly discuss the results of the HF methods. The spectra were calculated for the planar C_{2v} as well as the nonplanar C_2 form. The latter is the true minimum at the UBLYP/6-31G*, UHF/6-31G*, UMP2/6-31G*, and ROHF/6-31G* levels, but the geometry as well as the calculated frequencies and normal modes are changed only marginally when the symmetry is lowered.

Because resonance Raman spectra normally reveal only totally symmetric modes,[42] we will interpret the spectrum of DMA^+ using the modes that are totally symmetric in the planar C_{2v} geometry. As will be shown, this allows a straightforward assignment, so there is no need to invoke nontotally symmetric modes, including a_2 modes that become totally symmetric when the symmetry is lowered to C_2. The calculated frequencies are not scaled,[36,43] although a slightly better overall fit can be obtained by multiplying the frequencies by 1.006. The experimental data, shown in Figure 1, are available only for vibrational frequencies below ca. 1700 cm^{-1}, so the CH stretching region is not considered. The computed totally symmetric normal modes of the d_0 isotopomer are shown in Figure 2.

The frequency of the 8a mode is very well reproduced for all isotopomers. This mode is very characteristic for monosubstituted benzenes, essentially unperturbed by substituents.

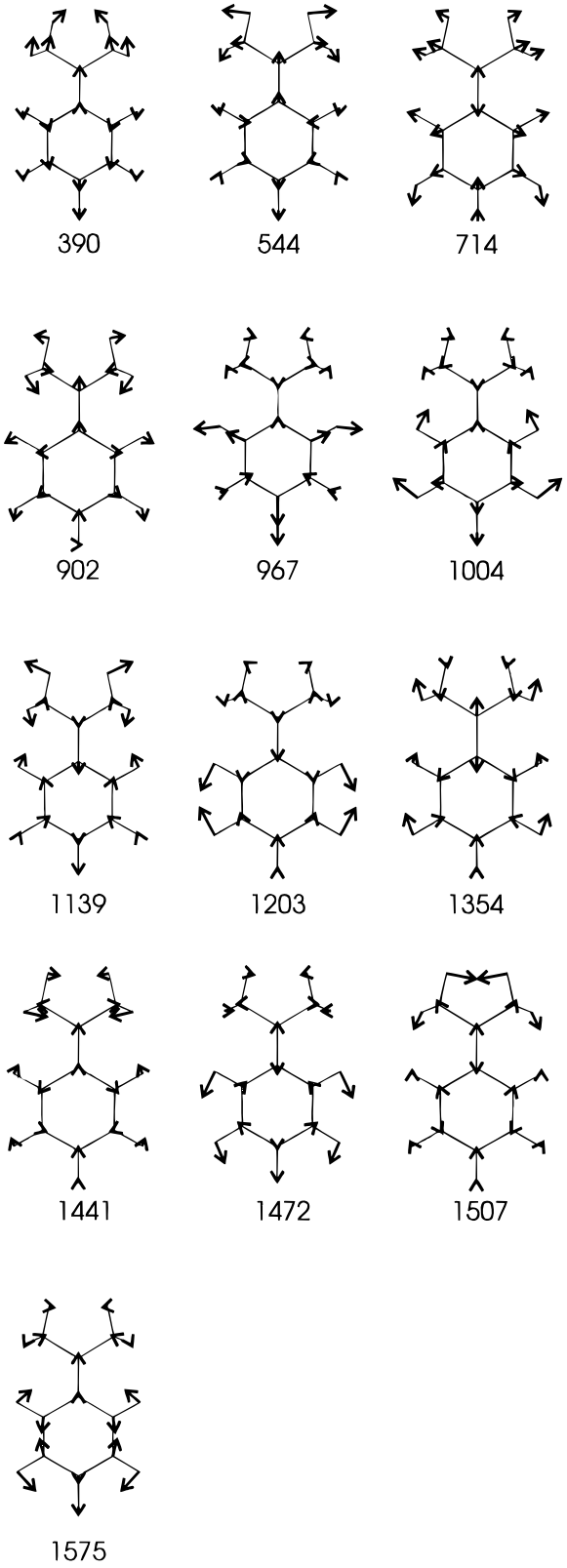

Figure 2. Representation of the totally symmetric normal modes of vibration of DMA^+ (C_{2v} point group) calculated at the UBLYP/6-31G* level.

Compared with the neutral molecule, the frequency is reduced by ca. 35 cm^{-1} for d_0 and d_6 and by 50 cm^{-1} in the ring-deuteriated isotopomers. The nature of this mode is a coupled C−C stretch and CCH bending, the contribution of the former being enhanced upon ionization.

The frequency of the second characteristic ring mode 19a is quite well reproduced for the d_0 and d_6 isotopomers. For the

ring-deuteriated analogs the frequency is shifted to a much lower value. Poizat and co-workers[22] assigned bands at 1387 cm^{-1} in d_5 and at 1397 cm^{-1} in d_{11} to the 19a vibration. As we show below, these are actually the N-ring stretching modes. It is noteworthy that mode 19a is not observed in the ring-deuteriated compounds (see section 4.4).

The frequency of the N-ring stretching vibration is sensitive to deuteriation of the ring and of the methyl groups. Changing the methyls into CD_3 is predicted to lead to a lowering of the frequency by ca. 10 cm^{-1}. Ring deuteriation, on the other hand, is predicted to lead to substantial increases in frequency of 22 and 31 cm^{-1} in d_5 and d_{11}, respectively. Experimentally, an increase in the frequency is found in all three deuteriated isotopomers: 21 cm^{-1} in d_5, 12 cm^{-1} in d_6, and 33 cm^{-1} in d_{11}. Thus, the observed effect of deuteriation of the methyl groups is not in agreement with the calculation, but the frequency increase upon ring deuteriation comes out nicely.

The observed and computed vibrational frequencies for ring modes 9a and 18a are in excellent agreement. In the ring-deuteriated isotopomers one of the two modes is not observed. The calculations indicate that this is mode 18a rather than 9a, as supposed by Poizat et al.[22]

The symmetric deformation of the methyl groups is computed at 1441 and 1447 cm^{-1} in the d_0 and d_5 isotopomers and at 1113 cm^{-1} in the methyl-deuteriated ones. The observed bands at 1474 cm^{-1} in d_5 and at 1130 cm^{-1} in d_{11} can be assigned to this vibration. For the parent isotopomer the band may coincide with the one observed at 1478 cm^{-1}. In the d_6 isotopomer it seems to remain unobserved. Poizat et al.[22] assign the bands at 1163 cm^{-1} in d_0 and at 1140 cm^{-1} in d_5 to the ρ_S(Me) vibration. According to our calculations the band at 824 cm^{-1} in d_6 can also be assigned in this way, rather than to an *N*-methyl stretching mode. On the basis of the calculation, ρ_S(Me) should appear at ca. 800 cm^{-1} in the d_{11} isotopomer, but it is not observed.

In the frequency region below 1000 cm^{-1} one finds the combinations of ring modes 12, 1, and 6a and the stretching and bending modes of the dimethylamino group. Experimentally only one of these has been observed for each isotopomer. For the d_0 compound the 735 cm^{-1} band has mainly ν(*N*-Me) character, and the band around 500 cm^{-1} (reported only for the deuteriated isotopomers) can be labeled "6a". Modes 1 and 12 tend to mix so strongly with other modes that they are hard to identify. In any case, mode 12 is not observed, and a band for mode 1 cannot be identified with certainty. The spectrum of DMA^+ (trace B in Figure 1) shows a feature near 900 cm^{-1}, but this is possibly a subtraction artifact due to the presence of a strong solvent band at 920 cm^{-1} and is therefore not listed as a band in Table 2. The intensity calculations (section 4.4), on the other hand, suggest that it may well be a real band, corresponding to ring mode 1.

We were surprised that mode 6a, expected near 544 cm^{-1}, was not reported for the parent isotopomer by the Poizat group.[22] We therefore remeasured the spectrum of the dimethylaniline radical cation and found a strong band at 536 cm^{-1}, which is obviously the band sought. It is still strange that the *N*-Me vibration is not seen in any of the deuteriated compounds.

Clearly, the DFT calculations account for the spectra remarkably well and lead convincingly to a revision of a few of the assignments. We shall now turn to the UHF and ROHF results.[44] The frequencies are uniformly scaled such that an optimal agreement is obtained for 26 bands of the four isotopomers. The scaling factors are 0.934 for UHF and 0.922 for ROHF.

On the whole, the agreement of the UHF calculated frequencies with experimental data is inferior to that obtained with the

TABLE 2: Calculated Harmonic Vibrational Frequencies (6-31G* Basis Set) of DMA^+ (C_{2v}) Compared with Experimental Data (A_1 Modes Only; Scaling Factors: 1.00 for UBLYP, 0.934 for UHF, 0.922 for ROHF, and 0.915 for CASSCF)

	d_0				d_6				d_5				d_{11}			
mode	BLYP	UHF	ROHF	CASSCF	obs[a]	BLYP	UHF	ROHF	CASSCF	obs[b]	BLYP	UHF	ROHF	CASSCF	obs[b]	BLYP	UHF	ROHF	CASSCF	obs[b]
8a	1575	1533	1588	1551	1568	1574	1538	1568	1540	1560	1535	1464	1572	1481	1528	1533	1467	1536	1484	1525
δ_A(Me)	1507	1563	1531	1524	n.o.	1064	1102	1097	1086	n.o.	1506	1558	1512	1540	n.o.	1063	1102	1098	1086	n.o.
19a	1472	1508	1468	1492	1478	1468	1504	1480	1487	1472	1268	1293	1290	1269	n.o.	1252	1281	1256	1257	n.o.
δ_S(Me)	1441	1495	1493	1474	n.o.[c]	1113	1158	1150	1141	n.o.	1447	1500	1485	1472	1474	1112	1158	1148	1140	1130
N-ring	1354	1421	1390	1421	1366	1344	1389	1367	1411	1378	1378	1434	1325	1442	1387	1375	1404	1309	1428	1397
9a	1203	1197	1219	1195	1203	1201	1195	1177	1191	1205	866	866	940	903	875	866	871	935	853	865
ρ_S(Me)	1139	1161	1133	1164	1163	800	815	819	806	824	1122	1145	1127	1149	1140	775	789	795	777	n.o.
18a	1004	1003	1003	985	1022	1017	1003	1003	984	1020	813	825	827	812	n.o.	835	847	857	837	n.o.
12	967	974	931	959	n.o.	962	944	826	928	n.o.	939	954	926	940	n.o.	937	1019	1014	927	n.o.
1	902	902	827	888	n.o.	997	1041	1037	1024	n.o.	902	905	763	845	n.o.	994	932	757	1005	n.o.
N-Me	714	719	712	705	735	690	695	686	681	n.o.	686	690	688	677	n.o.	667	671	667	658	n.o.
6a	544	540	540	533	536	499	496	495	490	490	538	534	534	527	534	493	490	490	485	487
NCN	390	393	389	388	n.o.	357	360	357	355	n.o.	385	388	384	382	n.o.	353	356	353	352	n.o.

[a] This work. n.o. means not observed. [b] Reference 22. [c] Probably coincident with 19a.

DFT calculations. The frequency of the 8a mode is consistently underestimated, especially in the ring-deuteriated isotopomers, while that of mode 19a is overestimated. Remarkably, for the d_0 and d_5 isotopomers the highest frequency computed mode in the spectral region of interest is in fact the asymmetric methyl deformation (not observed experimentally).

The frequency of the mode corresponding mostly to stretching of the N-ring bond is overestimated by more than 50 cm^{-1} in the d_0 and d_5 species and by a small amount in the methyl-deuteriated isotopomers. Thus, as with the DFT calculations, the shift to higher frequency upon methyl deuteriation is not reproduced.

The remaining observed bands in the resonance Raman spectra of DMA^+ and isotopomers can be adequately assigned using the UHF calculations, as well as with the DFT results.

According to the ROHF calculations the character of many of the modes is more complicated than according to the DFT calculations. The high-frequency 8a mode is so strongly mixed with methyl deformation and mode 19a that its nature can hardly be recognized in the parent isotopomer. According to the ROHF calculations, the modes observed at 875 and 865 cm^{-1} in d_6 and d_{11}, respectively, can be better assigned to 18a than to 9a. As discussed below, the ROHF results do not appear to be reliable. When the symmetry is lowered to C_2 a quite different electronic wave function is obtained and, not surprisingly, the computed vibrational spectrum also changes a lot, in contrast to the other cases discussed.

At the CASSCF level[45] the π-electron system was fully correlated (seven electrons in seven orbitals). The C_{2v} structure was found to be an energy minimum. The results of the CASSCF frequency calculations (scaling factor 0.915) are in better agreement with experiment than the UHF results but less satisfactory than those from the UBLYP calculations. Nevertheless, the CASSCF approach is important because it offers the only viable way to describe the potential energy surfaces of the resonant excited state of the radical cation, which is necessary for the prediction of the intensity pattern (section 4.4). Concerning the 8a mode, the frequency lowering upon deuteriation is strongly overestimated. This is because the contribution of the C−C stretching is too low relative to the contribution of the C−H bending deformations of the methyl groups and of the ring. In the counterpart of mode 8a, the 9a mode, the aromatic CH bending contribution is calculated a bit too small, as seen from the isotope shift in the d_5 species. The frequency of the 19a mode is somewhat overestimated. The N-ring stretching frequency is overestimated considerably, and the effects of deuteriation of the methyl group are not well reproduced. The remaining totally symmetric modes are calculated in agreement with experiment and with the UBLYP results.

3.3. Aniline Radical Cation. Encouraged by the results of the UBLYP calculations on the radical cation of DMA, we performed the same type of calculation also for the radical cation of aniline. The vibrational frequencies have been measured by means of resonance Raman spectroscopy of the relaxed radical cation in solution[20] and by ZEKE spectroscopy of the isolated molecule.[24] In the latter study, the frequencies were also computed at the UMP2/6-31G* level, but the results were rather disappointing. The UBLYP/6-31G* calculations (Table 3), on the other hand, match very well with the experimental data, even for the low-frequency region, where the harmonic approximation is questionable. For this species the C_{2v} structure corresponds to an energy minimum.

On the basis of our calculations (Table 3; a figure with normal modes and a table of calculated frequencies and assignments of the deuteriated isotopomers are available as supporting information) some of the assignments of Tripathi and Schuler[20] have to be revised. The bands at 1380 and 1494 cm^{-1} are due to the 19a mode and ν(N-ring) vibrations. Both modes are highly mixed, but the low-frequency band (1380 cm^{-1}) has more ν_{CN} character, while the one at higher frequency is a bit more like mode 19a. Ring deuteriation (cf. Table 2 and see supporting information) leaves almost all of the ν_{CN} character in the higher frequency mode, observed at 1455 and 1476 cm^{-1} in the d_5 and d_7 isotopomers, respectively. The weak band at 1458 cm^{-1} in the parent isotopomer must be attributed to a vibration of B_2 symmetry, gaining intensity through vibronic coupling, like the mode at 1338 cm^{-1} (calculated 1339 cm^{-1}). The nature of the 1458 cm^{-1} vibration is similar to mode 8b; the calculations suggest that the 1338 cm^{-1} vibration corresponds with mode 3, not 14 as inferred by Tripathi and Schuler. The benzene-like vibrations of B_2 symmetry are, however, heavily mixed, and the assignment of a Wilson symbol is quite arbitrary.

In the ZEKE experiments[24] several nontotally symmetric modes have been detected in the low-frequency region. Most of these can be readily assigned on the basis of the DFT calculation, although the symmetry assignments are not in all cases in agreement with those of Song et al. For the bands observed at 577 and 658 cm^{-1} there is no corresponding calculated mode.

TABLE 3: Results of UBLYP/6-31G* Calculations Compared with Experimental Data for Aniline Radical Cation[a]

mode	symmetry	frequency	RR (ref 20)	ZEKE (ref 24)
1 (γ_{CN})	b_1	182		179
2 (γ_{NH2})	a_2	354		356
3 (β_{CN})	b_2	371		
4 (16b)	b_1	438		445
5 (6a)	a_1	518	521	522
6 (γ_{NH2})	a_2	526		
7 (γ_{SNH2})	b_1	563		550 (b_2)
8 (6b)	b_2	581		581
9 (4)	b_1	619		629
10 (11)	b_1	768		
11 (10a)	a_2	780		790 (b_1)
12 (1)	a_1	802	820	814
13 (17b)	b_1	904		
14 (17a)	a_2	953		
15 (12)	a_1	967	no	
16 (5)	b_1	978		
17 (18a)	a_1	986	1001	996
18 (β(as)$_{NH2}$)	b_2	1002		
19 (9b)	b_2	1108		
20 (18b)	b_2	1170		
21 (9a)	a_1	1188	1175	1188
22 (3)	b_2	1339	1338	
23 (7a = ν(N-ring)/19a)	a_1	1361	1380	1385
24 (14)	b_2	1365		
25 (8b)	b_2	1437	1458	
26 (19a/7a)	a_1	1478	1494	1478
27 (19b)	b_2	1510		
28 (8a)	a_1	1589	1574	1594
29 (β(S)$_{NH2}$)	a_1	1648	n.o.	

[a] Only modes below 1700 cm^{-1} are reported. Labels correspond approximately to those of ref 35.

4. Computed Molecular Structures, Wave Functions, and Potential Energy Surfaces

In this section we shall discuss the molecular structures of DMA and its radical cation as computed at different levels of approximation, and we shall compare these with experimental data other than vibrational spectra. Furthermore, a brief description of the characteristic features of the electronic wave

TABLE 4: Computed Geometric Features of DMA, DMA$^+$, and Aniline Radical Cation[a]

species	method	E (Hartree)	r_{CN}	r_{NMe}	r_{12}	r_{23}	r_{34}	τ
DMA, C_s	HF	−363.78039	1.394	1.447	1.401	1.383	1.384	26.3[b]
DMA$^+$ C_{2v}	UHF	−363.57798	1.336	1.477	1.435	1.382	1.409	0
DMA$^+$ C_2	UHF	−363.57808	1.336	1.475	1.435	1.382	1.407	8.5
DMA$^+$ C_{2v}	ROHF	−363.54924	1.322	1.471	1.439	1.360	1.404	0
DMA$^+$ Cc_2	ROHF	−363.54923	1.376	1.466	1.408	1.375	1.391	14.9
DMA$^+$ C_{2v}	UMP2	−364.68853	1.330	1.469	1.433	1.351	1.401	0
DMA$^+$ C_2	UMP2	−364.68865	1.330	1.468	1.432	1.531	1.401	8.3
DMA$^+$ C_{2v}	UBLYP	−365.78866	1.375	1.484	1.442	1.389	1.418	0
DMA$^+$ C_2	UBLYP	−365.78884	1.374	1.482	1.442	1.390	1.417	10.4
DMA$^+$ C_{2v}	CASSCF 1^2B_1	−363.63534	1.327	1.478	1.443	1.376	1.410	0
DMA$^+$ C_{2v}	CASSCF 1^2A_2	−363.56907	1.339	1.461	1.417	1.441	1.388	0
DMA$^+$ C_{2v}	CASSCF 2^2B_1	−363.52914	1.414	1.462	1.438	1.372	1.442	0
aniline$^+$	UBLYP	−287.21307	1.351		1.445	1.385	1.425	0

[a]Basis set 6-31G* for all methods. MP2 calculations with frozen core. Bonds lengths in angstroms, dihedral angle τ = C(Me)−N−C1−C2 in degrees. [b] In this case τ is the pyramidalization angle.

function in DMA and in the lowest electronic states of the radical cation will be given. Finally, we will present the estimation of resonance Raman intensities as derived from the potential energy surfaces of the resonant states.

4.1. Molecular Structures. In Table 4 are listed the energies and most important geometric features of the optimized structures at various levels of theory. In the neutral dimethylaniline the amino group was found to be pyramidal; in the radical cations it was planar, as was the benzene ring. In the structures of C_2 symmetry there was a small torsion (τ) around the C_1−N bond.

For investigations of the potential energy surface of the excited states of the radical cations the CASSCF method is at present the most appropriate. For these calculations we have limited the system to C_{2v} symmetry. The ground state of DMA$^+$ is of B_1 symmetry; the lowest excited state is 1^2A_2. The resonant state in the Raman experiments is the second excited state 2^2B_1.

Limited experimental structural data are available for DMA. From electron diffraction data it was concluded that the structure has C_s symmetry.[46] The C_1−N bond length was found to be 1.43 ± 0.02 Å, the *N*-methyl bond length was 1.46 Å, and the average CNC bond angle was 116°. Our calculations give an average angle of 117.6°. In the gas phase the amino group was found to be pyramidal, with an out-of-plane angle of 27°,[47] which is very well reproduced by the calculated value of 26.3°. In the Cambridge Structural Database[48] we found 10 4-alkyl-DMA derivatives, in which the C_1−N bond lengths varied between 1.36 and 1.40 Å. Pyramidalization was in most cases significantly smaller than in the gas phase, and the dimethylamino group was twisted only slightly with respect to the plane of the benzene ring. Effects of crystal-packing forces on dihedral angles are common,[49] but in this case the low inversion barrier[47] also allows flattening of the amino group due to intermolecular interactions in the solid state. The HF/6-31G* level is known to be generally adequate for the calculation of the structures of organic molecules.[38] In the case of amines the polarization functions are essential.[50,51] Previous calculations found a twisted optimized structure for DMA at the 3-21G(N*) level.[52] Gorse and Pesquer[53] reported that DMA has two minimum-energy structures (C_s and C_1) at the HF/6-31G* level, but they gave no details other than the pyramidalization angle. We found the C_1 structure to have essentially the same energy as the C_s structure, at both HF/6-31G* and MP2/6-31G* levels of theory. This agrees with the notion that the potential energy surface for twisting and pyramidalization is very shallow. Important for our purpose is that the optimized 6-31G* C_s structure (Table 4) is in good agreement with the known

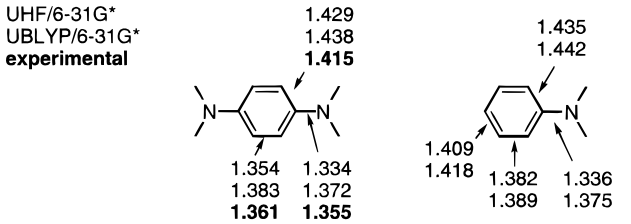

Figure 3. Comparison of bond lengths according to UHF and UBLYP calculations of the radical cations of TMPD and DMA. For TMPD radical cation the experimental bond lengths are included in boldface. Experimental data are from ref 55.

experimental structures and can account for the vibrational spectra.

Going from the neutral molecule to the radical cation, the bond between the nitrogen atom and the aromatic ring (r_{CN}) is considerably shortened. According to UHF, UMP2, and CASSCF calculations, $r_{CN} \approx 1.33$ Å, while the DFT calculation predicts a bond length of 1.375 Å. With the ROHF method a large difference in the bond lengths is found between the optimized planar C_{2v} and the twisted C_2 forms. This unexpected result was verified using a different program, viz. GAMESS-UK.[54] It was possible by taking small steps along the out-of-plane coordinate, and optimizing all other degrees of freedom, to find a range of torsion angles in which both structures, i.e., the "long-bond" and the "short-bond", coexisted. This phenomenon is most likely due to a HF instability of the ROHF wave function, but unfortunately the programs do not provide facilities for testing this.

For the radical cations experimental structural data are not available. The related *N*,*N*,*N*,*N*-tetramethyl-*p*-phenylenediamine (TMPD) forms radical cation salts that could be studied by means of X-ray crystallography.[55,56] The experimental data could be reasonably well reproduced with UHF/3-21G calculations.[27] This, however, does not imply that the same level of theory is also appropriate for the simple aniline radical cations, because spin contamination played a much smaller role in the case of phenylenediamines (see below). The CN bond in TMPD is shortened upon one-electron oxidation by ca. 0.06 Å.[55−57] The computed bond lengths of the radical cation of TMPD using UHF/6-31G* and UBLYP/6-31G* are compared in Figure 3.

For TMPD the UHF values of the bond lengths in the π-system are in somewhat better agreement with experiment than the UBLYP values, although both are quite acceptable. The UBLYP bond lengths are systematically too large, in line with observations for neutral molecules.[43] The computed CN bond has essentially the same length in DMA$^+$ as in the TMPD radical cation. The experimental equilibrium bond lengths fall in between the UHF and UBLYP values, suggesting that perhaps

TABLE 5: Some Characteristics of the Electronic Wave Functions: Natural Atomic Population Charges, Mulliken Spin Density on N, and Expectation Value of the S^2 Operator for Radical Cations

species	level	N	C1	C2,6	C3,5	C4	ρ_N	$<S^2>$
DMA								
C_s	HF	−0.54	0.23	−0.30	−0.18	−0.28		
DMA^+								
C_{2v}	UHF	−0.21	0.23	−0.20	−0.20	−0.15	0.72	1.29
C_2	UHF	−0.21	0.23	−0.20	−0.20	−0.14	0.72	1.29
C_{2v}	ROHF	−0.36	0.30	−0.19	−0.23	−0.04	0.24	
C_2	ROHF	−0.15	0.10	−0.17	−0.23	−0.11	0.63	
C_{2v}	UMP2	−0.34	0.27	−0.21	−0.23	−0.06	0.21	1.21
C_2	UMP2	−0.33	0.27	−0.21	−0.23	−0.06	0.22	1.21
C_{2v}	UBLYP	−0.22	0.19	−0.20	−0.21	−0.12	0.42	0.76
C_2	UBLYP	−0.22	0.19	−0.20	−0.20	-0.12	0.42	0.76
C_{2v}	CASSCF 1^2B_1	−0.23	0.25	−0.20	−0.20	−0.12	0.29	
C_{2v}	CASSCF 1^2A_2	−0.39	0.45	−0.08	−0.35	−0.11	0.11	
C_{2v}	CASSCF 2^2B_1	−0.14	0.25	−0.29	−0.14	−0.13	0.18	
$aniline^+$	UBLYP	−0.61	0.22	−0.19	−0.20	−0.09	0.35	0.76

a mixed HF/DFT calculation[58] may give even better results. Preliminary calculations and some very recent studies of others support this idea.[59]

4.2. Nature of the Electronic Wave Functions. In Table 5 we report some characteristics of the electronic wave functions. The natural atomic populations[60] can be used as a measure of the charge transfer between the amino group and the benzene ring. The spin density on the nitrogen atom in DMA^+, ρ_N, can be compared with the experimental estimate of ca. 50%.[11] The UBLYP calculations reproduce this quite well. The expectation value of S^2 should be 0.75 for a doublet state. The much higher values for the UHF-based methods indicate serious spin contamination. The DFT calculations do not suffer from this problem, even though they are also unrestricted.

The qualitative pattern of the charge distribution is similar in all methods. The difference between the radical cation and the neutral molecule occurs in particular at the nitrogen atom and the ortho- and para-ring atoms, as expected. There is quite a big difference between the charges in the radical cations of aniline and DMA.

4.3. Excited States. The relaxed energies of the two lowest excited states of DMA^+ as calculated at the CASSCF level are reported in Table 4. The vertical excitation energies at the geometry of the ground state are 2.12 eV (corresponding to absorption at 586 nm) and 3.12 eV (397 nm) for the 1^2A_2 and 2^2B_1 states, respectively. The former corresponds with the broad absorption band in the red with a maximum around 2 eV;[16] the latter corresponds with the resonant state in our experiments, with an absorption maximum at 465 nm. Considering the fact that dynamical correlation effects are neglected in the calculations, the agreement between calculated and experimental excitation energies is very satisfactory.

A qualitative sketch of the π molecular orbitals of DMA^+ is presented in Figure 4. Note that in the CASSCF calculations significant mixing of these idealized "basis orbitals" takes place, depending on the orbital occupation. This affects in particular the π_2 and π_4 orbitals.

The configuration $1b_1^2 2b_1^2 3a_2^2 4b_1^1 5a_2^0 6b_1^0 7b_1^0$ dominates the wave function of the ground state of the radical cation, although there is a noticeable admixture (coefficients between 0.1 and 0.15) of three excited configurations. The bond length pattern (Table 4) is consistent with a quinoidal electronic structure. The lowest excited state 1^2A_2 is dominated by the configuration in which one electron is promoted from π_3 to π_4. Again, several configurations mix into the CASSCF expansion with coefficients

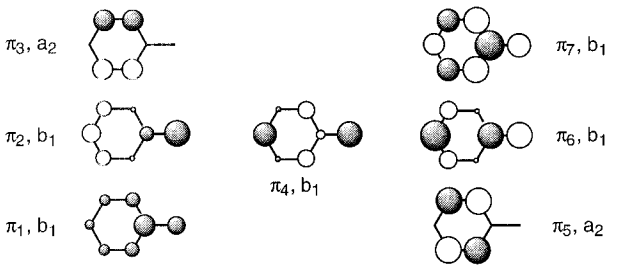

Figure 4. Schematic representation of the π-MOs of DMA^+. The coefficients are from the MOs from a state-averaged CASSCF calculation involving the three lowest roots with equal weights.

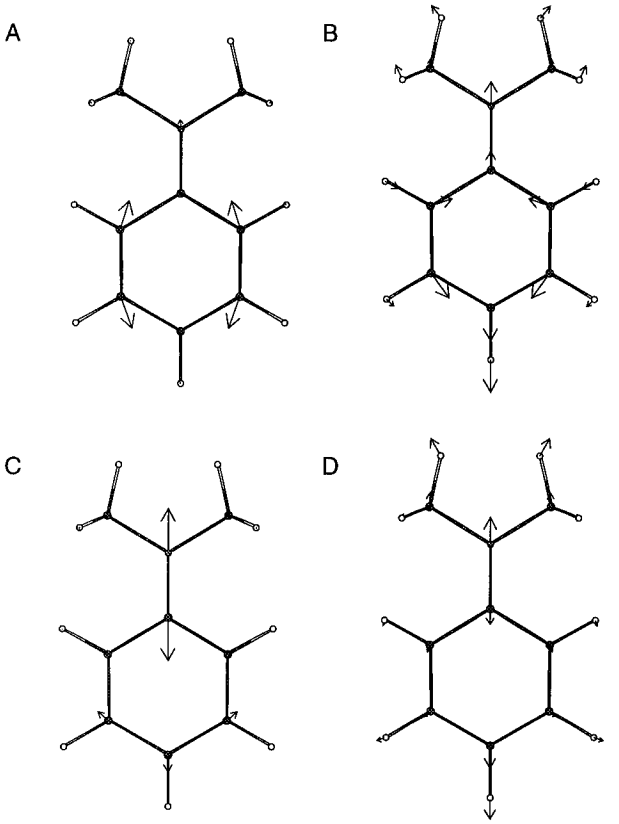

Figure 5. Gradient and displacement vectors of DMA^+ in the excited states: (A) gradient in the $1A_2$ state: (B) displacement in the $1A_2$ state; (C) gradient in the $2B_1$ state; (D) displacement in the $2B_1$ state. The geometry is that of the ground state. The lengths of the arrows represent the gradient in Hartree/Bohr (scaled 10×) or the displacement in angstroms (scaled 10×).

between 0.1 and 0.2. Compared with the 1^2B_1 state, the 1^2A_2 state shows an increased polarization of the CN bond and a transfer of charge from the ring to the amino group. The reduced occupation of π_3 is also reflected in a lengthening of the C2−C3 and C5−C6 bonds and an increase in the bond order between C2 and C6 and between C3 and C5. This leads to distortion of the ring, with the angle C2−C1−C6 being only 114.7°. Changes in the geometry following excitation, as well as the gradients in the 1^2A_2 and 2^2B_1 vertically excited states are represented in Figure 5.

The second B_1 state is mostly a mixture of two singly excited configurations ($0.77 \times |\pi_2 \rightarrow \pi_4| - 0.48 \times |\pi_4 \rightarrow \pi_6|$) but doubly excited configurations are also significant. As can be derived from the orbital occupation in the leading configurations, the bonding between C1 and N is weaker in 2^2B_1 than in 1^2B_1, which results in a considerable lengthening of the C−N bond (see Table 4). Upon geometry optimization of the 2^2B_1 state this becomes lower in energy than the 1^2A_2 state.

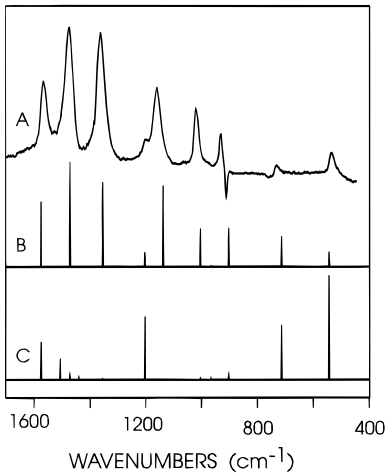

Figure 6. Intensity patterns calculated for the Raman spectra of DMA^+ in resonance with the transitions from the $^2B_1$ ground state to the 2^2B_1 state (B) and the 1^2A_2 state (C). For comparison, the experimental spectrum is included (A).

4.4. Resonance Raman Intensities. For the totally symmetric modes *A*-term scattering is most likely to be the dominant contribution to the resonance Raman intensities.[42] Theory shows that the intensity is approximately proportional to a sum over Franck−Condon factors. Assuming that the normal modes are the same in the two states involved, it can be shown that the intensity of the band corresponding to mode k is proportional to the square of the dimensionless displacement parameters (eq 1).[42,61]

$$I_k \propto \omega(\Delta \mathbf{x}_k \mathbf{M}^{1/2} \mathbf{L}_k)^2 \quad (1)$$

The assumption that the frequency of the vibrations does not change allows the Cartesian displacement $\Delta \mathbf{x}_k$ to be computed directly from the gradient **g** of the excited state surface at the ground state geometry.[61] This leads to eq 2.

$$I_k \propto \omega_k^{-3}(\mathbf{g}\mathbf{M}^{-1/2}\mathbf{L}_k)^2 \quad (2)$$

The intensity of the totally symmetric vibrations of DMA^+ was calculated according to eqs 1 and 2 by taking the displacement vector or the gradient vector from the CASSCF calculations and using either the UBLYP or the CASSCF normal modes. The best agreement with experiment was found when the CASSCF normal modes were used in combination with the computed displacement in the 2^2B_1 excited state. These intensities, which show a very satisfactory agreement with experiment, are shown in Figure 1. The calculations are consistent with the fact that the 19a vibration is not observed in the ring-deuteriated isotopomers. Apparently, mode 19a derives most of its intensity from mixing with ν(N-ring).

In Figure 6 a comparison is made of the estimated intensities for the 1^2A_2 state and the 2^2B_1 state. The intensity pattern for the B_1 to A_2 transition shows large resonance enhancement for the 9a, ν(N-methyl), and 6a modes, with relatively little intensity in the N-ring stretching and 19a modes. This is distinctly different from the pattern observed for the 2^2B_1 state. The difference can be qualitatively understood by inspection of Figure 5, which shows that the N-ring bond length barely changes upon transition to the 1^2A_2 state, while the ring distortion projects strongly onto the 6a mode.

5. Discussion

A key vibration of the aniline derivatives is obviously the N-ring stretching mode. One would expect this mode to be sensitive to changes in the electronic structure of the molecule. Indeed, in going from the neutral molecule to the radical cation, the frequency increases in DMA by ca. 30 cm^{-1} as a result of the increased double-bond character, as argued by Poizat et al.[22] In contrast, all other ring modes shift to a lower frequency. The increased C−N bond order is also reflected in the considerable decrease of the bond length, 0.06 Å, according to our estimate based on comparison with tetramethyl-*p*-phenylenediamine. For the aniline molecule the frequency of the N-ring stretching mode increases from 1279 cm^{-1} (ref 35) in the neutral molecule to 1380 cm^{-1} in the radical cation. According to our calculations the bond lengths are the same in DMA and aniline, but the C−N bond is 0.02 Å shorter in $aniline^+$ than in DMA^+. The *N*-methyl groups somewhat attenuate the changes in the structure and vibrations of aniline upon ionization. For an analogous π-system, the phenoxyl radical, the observation was made that the CO bond was computed to be as short as a double bond, while the stretching force constant was intermediate between those of CO single and double bonds.[28] Thus, a simple relationship between electronic structure, bond length, and vibrational frequency should not be expected to exist in this case.

The best prediction of the frequency of the N-ring vibration comes from the UBLYP calculations. The CASSCF calculations, which are quite good for most other modes, overestimate the frequency by as much as 55 cm^{-1} in the parent isotopomer. The N-ring stretching in DMA and DMA^+ is a complex normal mode, and its nature changes substantially upon deuteriation. In the graphical representation (Figure 2) contributions from methyl deformation and the CH bending mode 19a are clearly recognized. In spite of this complexity our calculations predict that ^{15}N isotopic substitution would only affect the frequency of the ν(N-ring) mode ($\Delta\nu = -17$ cm^{-1}) and the ν(*N*-Me) vibration ($\Delta\nu = -6$ cm^{-1}), but not other modes such as 19a. Unfortunately, there are no experimental data for [^{15}N]DMA, but for the case of *N*-phenylpiperidine[29] an analogous prediction is borne out by experiment. Thus, the isotopic frequency shift may be taken as an experimental criterion for labeling the ν-(N-ring) vibration where the graphical display of the mode seems less characteristic.

The isotope effects on the N-ring vibration in DMA^+ can be qualitatively explained. Deuteriation of the ring shifts the 19a mode from a frequency above that of ν(N-ring) to one below it. As a result, the N-ring mode is shifted to higher frequency. This effect is reproduced by the calculations (except ROHF). Inspection of the normal modes also shows the diminished mixing-in of mode 19a in the N-ring mode in the d_5 isotopomer and a reversal of the sign of the contribution. The effect of methyl deuteriation can be analogously explained, although the situation is more complicated because all three symmetric combinations of the deformation modes mix. We note, however, that in d_0 and d_5 two of them are at higher frequency than ν(N-ring), while in the d_6 and d_{11} compounds all methyl deformation modes have a lower frequency than the N-ring vibration. Unfortunately, this detail is not correctly reproduced by any of the calculations.

According to the HF calculations for the neutral DMA molecule the N-ring stretching mode is even more mixed than in the radical cation, and its response to deuteriation is quite different. In the ring-deuteriated isotopomers the mixing with mode 19a is so strong that the simple labels lose their meaning.

6. Conclusions

The resonance Raman spectrum of DMA^+ has been successfully analyzed on the basis of UBLYP/6-31G* and π-space

CASSCF/6-31G* calculations. The latter are less accurate for the vibrational frequencies but permit the calculation of the excitation energies and the potential energy surfaces of the two relevant lowest excited states of DMA^+. The excitation energies are in good agreement with experiment, and the same is true for the intensities derived from the excited state displacements. This suggests that the CASSCF calculations give an essentially correct description of the excited state potential energy surfaces. The UBLYP calculations also account very well for the vibrational frequencies of the radical cation of aniline. It appears that the area of molecular structure and vibrational spectra of organic radical cations forms another domain where the gradient-corrected DFT methodology can be applied very successfully.[59,62−65]

The N-ring stretching vibration is in all cases a complex vibration, with various local modes contributing. The UBLYP calculations predict its frequency best. It is perhaps not surprising that there is still a discrepancy between this calculation and experiment as concerns the effect of methyl deuteriation on the frequency. We have used the computed force constants as they are, without any scaling. A better agreement can undoubtedly be found by developing a scaled quantum mechanical force field,[28,36] with different scaling factors for the force constants for different kinds of local coordinates, but this is not the objective of the present research. Given the high quality of the DFT results, we prefer to have more generality by using the ab initio data as they are, even if this is at the expense of accuracy.

For the neutral DMA molecule HF/6-31G* was found to be an appropriate level of theory, in line with general experience. In this case density functional methods may perform slightly better[36] and will be especially useful when IR intensities are concerned,[36,63] but they are (at present) computationally less efficient.

The lowest triplet state of DMA appears to be an inefficient Raman scatterer, even though its optical absorption properties are very similar to those of the radical cation. This is in contrast with substituted derivatives, which do give good resonance Raman spectra.[21,29]

Work on related systems (*N*-phenylpiperidine, *N*-phenylmorpholine, *N*-phenylpyrrolidine) is in progress.[29] The experience gained in the present study shows that some of the normal modes of vibration are rather complex and can be expected to depend on details of the molecular structure and on isotopic substitution, which will make it necessary to perform the same types of calculation on these larger molecules.

Acknowledgment. We thank John van Ramesdonk, Frans Langkilde, and Krzysztof Bajdor for help with the experiments, Mike Robb for advice concerning the CASSCF calculations, Wybren-Jan Buma for helpful discussions, and Francesco Zerbetto for providing us with a computer program for the calculation of resonance Raman intensities according to eq 2. This research was sponsored by the Stichting Nationale Computer Faciliteiten (National Computing Facilities Foundation, NCF) for the use of supercomputer facilities and supported (in part) by the Netherlands Foundation for Chemical Research (SON), with financial support from the Nederlandse Organisatie voor Wetenschappelijk Onderzoek (Netherlands Organization for Scientific Research, NWO). In addition, NWO provided a travel grant to A.M.B., which has been essential in the initiation of this work. We gratefully acknowledge grants from the Danish Natural Science Research Council to the Center of Molecular Dynamics and Laser Chemistry.

Supporting Information Available: Figure showing the totally symmetric normal modes of the aniline radical cation, calculated at the UBLYP/6-31G* level and a table with the observed and calculated frequencies for the isotopomers of $aniline^+$ (6 pages). Ordering information is given on any current masthead page.

References and Notes

(1) Leonhardt, H.; Weller, A. *Z. Phys. Chem. (Munich)* **1961**, *29*, 277.
(2) Leonhardt, H.; Weller, A. *Ber. Bunsen-Ges. Phys. Chem.* **1963**, *67*, 791.
(3) Schneider, S.; Geiselhart, P.; Seel, G.; Lewis, F. D.; Dykstra, R. E.; Nepras, M. J. *J. Phys. Chem.* **1989**, *93*, 3112.
(4) Rettig, W.; Haag, R.; Wirz, J. *Chem. Phys. Lett.* **1991**, *180*, 216.
(5) Brouwer, A. M.; Mout, R. D.; Maassen van den Brink, P. H.; van Ramesdonk, H. J.; Verhoeven, J. W.; Jonker, S. A.; Warman, J. M. *Chem. Phys. Lett.* **1991**, *186*, 481.
(6) Brouwer, A. M.; Eijckelhoff, C.; Willemse, R. J.; Verhoeven, J. W.; Schuddeboom, W.; Warman, J. M. *J. Am. Chem. Soc.* **1993**, *115*, 2988.
(7) Scherer, T.; van Stokkum, I. H. M.; Brouwer, A. M.; Verhoeven, J. W. *J. Phys. Chem.* **1994**, *98*, 10539.
(8) Willemse, R. J.; Verhoeven, J. W.; Brouwer, A. M. *J. Phys. Chem.* **1995**, *99*, 5753.
(9) Brouwer, A. M.; Langkilde, F. W.; Bajdor, K.; Wilbrandt, R. *Chem. Phys. Lett.* **1994**, *225*, 386.
(10) Parker, V. D.; Tilset, M. *J. Am. Chem. Soc.* **1991**, *113*, 8778.
(11) Rao, D. N. R.; Symons, M. C. R. *J. Chem. Soc., Perkin Trans. 2* **1985**, 991.
(12) Goez, M. *Z. Phys. Chem. (Munich)* **1990**, *169*, 123.
(13) Goez, M. *Z. Phys. Chem. (Munich)* **1990**, *169*, 133.
(14) Land, E. J.; Richards, J. T.; Thomas, J. K. *J. Phys. Chem.* **1972**, *76*, 3805.
(15) Zador, E.; Warman, J. M.; Hummel, A. *J. Chem. Soc., Faraday Trans. 1* **1976**, *72*, 1368.
(16) Shida, T.; Nosaka, Y.; Kato, T. *J. Phys. Chem.* **1978**, *82*, 695.
(17) Shida, T. *Electronic Absorption Spectra of Radical Ions*; Elsevier: Amsterdam, 1988.
(18) Forster, M.; Hester, R. E. *J. Chem. Soc., Faraday Trans. 2* **1981**, *77*, 1535.
(19) Hester, R. E.; Williams, K. P. J. *J. Chem. Soc., Perkin Trans. 2* **1982**, 559.
(20) Tripathi, G. N. R.; Schuler, R. H. *J. Chem. Phys.* **1987**, *86*, 3795.
(21) Poizat, O.; Bourkba, A.; Buntinx, G.; Deffontaine, A.; Bridoux, M. *J. Chem. Phys.* **1987**, *87*, 6379.
(22) Poizat, O.; Guichard, V.; Buntinx, G. *J. Chem. Phys.* **1989**, *90*, 4697.
(23) Guichard, V.; Bourkba, A.; Poizat, O.; Buntinx, G. *J. Phys. Chem.* **1989**, *93*, 4429.
(24) Song, X.; Yang, M.; Davidson, E. R.; Reilly, J. P. *J. Chem. Phys.* **1993**, *99*, 3224.
(25) Kim, B.; Weber, P. M. *J. Phys. Chem.* **1995**, *99*, 2583.
(26) Langkilde, F. W.; Bajdor, K.; Wilbrandt, R.; Negri, F.; Zerbetto, F.; Orlandi, G. *J. Chem. Phys.* **1994**, *100*, 3503.
(27) Chipman, D. M.; Sun, Q.; Tripathi, G. N. R. *J. Chem. Phys.* **1992**, *97*, 8073.
(28) Chipman, D. M.; Liu, R.; Zhou, X.; Pulay, P. *J. Chem. Phys.* **1994**, *100*, 5023.
(29) Brouwer, A. M.; Wiering, P. G.; van Ramesdonk, H. J.; Langkilde, F. W.; Bajdor, K.; Wilbrandt, R. Unpublished results.
(30) Previtali, C. M. *J. Photochemistry* **1985**, *31*, 233.
(31) Murov, S. L.; Carmichael, I.; Hug, G. L. *Handbook of Photochemistry*; Dekker: New York, 1993.
(32) Shimanori, H.; Sato, A. *J. Phys. Chem.* **1994**, *98*, 13481.
(33) Guichard, V.; Bourkba, A.; Lautie, M.-F.; Poizat, O. *Spectrochim. Acta A* **1989**, *45A*, 187.
(34) Perrier-Datin, A.; Lebas, J. M. *J. Chim. Phys.* **1972**, 591.
(35) Castellá-Ventura, M.; Kassab, E. *Spectrochim. Acta* **1994**, *50A*, 69.
(36) Rauhut, G.; Pulay, P. *J. Phys. Chem.* **1995**, *99*, 3093.
(37) Frisch, M. J.; Head-Gordon, M.; Trucks, G. W.; Foresman, J. B.; Schlegel, H. B.; Raghavachari, K.; Robb, M.; Binkley, J. S.; Gonzalez, C.; Defrees, D. J.; Fox, D. J.; Whiteside, R. A.; Seeger, R.; Melius, C. F.; Baker, J.; Martin, R. L.; Kahn, L. R.; Stewart, J. J. P.; Topiol, S.; Pople, J. A. *Gaussian 90*; Gaussian, Inc.: Pittsburgh, PA, 1990.
(38) Hehre, W. J.; Radom, L.; von R. Schleyer, P.; Pople, J. A. *Ab Initio Molecular Orbital Theory*; Wiley: New York, 1986.
(39) Frisch, M. J.; Trucks, G. W.; Schlegel, H. B.; Gill, P. M. W.; Johnson, B. G.; Wong, M. W.; Foresman, J. B.; Robb, M. A.; Head-Gordon, M.; Replogle, E. S.; Gomperts, R.; Andres, J. L.; Raghavachari, K.; Binkley, J. S.; Gonzalez, C.; Martin, R. L.; Fox, D. J.; Defrees, D. J.; Baker, J.; Stewart, J. J. P.; Pople, J. A. *Gaussian 92/DFT*; Gaussian, Inc.: Pittsburgh, PA, 1993.
(40) Becke, A. D. *Phys. Rev. A* **1988**, *38*, 3098.

(41) Lee, C.; Yang, W.; Parr, R. G. *Phys. Rev. B* **1988**, *37*, 785.
(42) Clark, R. J. H.; Dines, T. J. *Angew. Chem., Int. Ed. Engl.* **1986**, *25*, 131.
(43) Johnson, B. G.; Gill, P. M. W.; Pople, J. A. *J. Chem. Phys.* **1993**, *98*, 5612.
(44) For these calculations Gaussian 92 was used: Frisch, M. J.; Trucks, G. W.; Head-Gordon, M.; Gill, P. M. W.; Wong, M. W.; Foresman, J. B.; Johnson, B. G.; Schlegel, H. B.; Robb, M. A.; Replogle, E. S.; Gomperts, R.; Andres, J. L.; Raghavachari, K.; Binkley, J. S.; Gonzalez, C.; Martin, R. L.; Fox, D. J.; Defrees, D. J.; Baker, J.; Stewart, J. J. P.; Pople, J. A. *Gaussian 92*; Gaussian, Inc.: Pittsburgh, PA, 1992.
(45) These calculations could be successfully performed with Gaussian 94: Frisch, M. J.; Trucks, G. W.; Schlegel, H. B.; Gill, P. M. W.; Johnson, B. G.; Robb, M. A.; Cheeseman, J. R.; Keith, T.; Petersson, G. A.; Montgomery, J. A.; Raghavachari, K.; Al-Laham, M. A.; Zakrzewski, V. G.; Ortiz, J. V.; Foresman, J. B.; Cioslowski, J.; Stefanov, B. B.; Nanayakkara, A.; Challacombe, M.; Peng, C. Y.; Ayala, P. Y.; Chen, W.; Wong, M. W.; Andres, J. L.; Replogle, E. S.; Gomperts, R.; Martin, R. L.; Fox, D. J.; Binkley, J. S.; Defrees, D. J.; Baker, J.; Stewart, J. J. P.; Head-Gordon, M.; Gonzalez, C.; Pople, J. A. *Gaussian 94*; Gaussian, Inc.: Pittsburgh, PA, 1995.
(46) Vilkov, L. V.; Timasheva, T. P. *Proc. Acad. Sci. USSR* **1965**, *161*, 261.
(47) Cervellati, R.; Borgo, A. D.; Lister, D. G. *J. Mol. Struct.* **1982**, *78*, 161.
(48) Allen, F. H.; Kennard, O. *Chem. Des. Autom. News* **1993**, *8*, 31.
(49) Brock, C. P.; Minton, R. P. *J. Am. Chem. Soc.* **1989**, *111*, 4586.
(50) Niu, Z.; Boggs, J. E. *J. Mol. Struct. (THEOCHEM)* **1984**, *109*, 381.
(51) Bock, C. W.; George, P.; Trachtman, M. *Theor. Chim. Acta* **1986**, *69*, 235.
(52) Ando, K.; Kato, S. *J. Chem. Phys.* **1991**, *95*, 5966.
(53) Gorse, A. D.; Pesquer, M. *J. Mol. Struct. (THEOCHEM)* **1993**, *281*, 21.
(54) Guest, M. F.; Fantucci, P.; Harrison, R. J.; Kendrick, J.; van Lenthe, J. H.; Schoeffel, K.; Sherwood, P. *GAMESS-UK*; Computing For Science: Warrington, U.K., 1993.
(55) de Boer, J. L.; Vos, A. *Acta Crystallogr.* **1972**, *B28*, 835.
(56) de Boer, J. L.; Vos, A. *Acta Crystallogr.* **1972**, *B28*, 839.
(57) Ikemoto, I.; Katagiri, G.; Nishimura, S.; Yakushi, K.; Kuroda, H. *Acta Crystallogr., Sect. B* **1979**, *35*, 2264.
(58) Becke, A. D. *J. Chem. Phys.* **1993**, *98*, 5648.
(59) Qin, Y.; Wheeler, R. A. *J. Chem. Phys.* **1995**, *102*, 1689.
(60) Reed, A.; Weinstock, R. B.; Weinhold, F. *J. Chem. Phys.* **1985**, *83*, 735.
(61) Negri, F.; Orlandi, G.; Zerbetto, F.; Zgierski, M. Z. *J. Chem. Phys.* **1995**, *103*, 5911.
(62) Eriksson, L. A.; Lunell, S.; Boyd, R. J. *J. Am. Chem. Soc.* **1993**, *115*, 6896.
(63) Ho, Y. P.; Yang, Y.; Klippenstein, S. J.; Dunbar, R. J. *J. Phys. Chem.* **1995**, *99*, 12115.
(64) Keszthelyi, T.; Wilbrandt, R.; Bally, T. *J. Phys. Chem.* **1996**, submitted for publication.
(65) Keszthelyi, T.; Wilbrandt, R.; Bally, T.; Roulin, J. L. *J. Phys. Chem.* **1996**, submitted for publication.

JP960013S